

Tidal deformability of dark matter clumps

Raissa F. P. Mendes¹ and Huan Yang^{2,3}

¹*Department of Physics, University of Guelph, Guelph, Ontario, N1G 2W1, Canada*

²*Perimeter Institute for Theoretical Physics, Waterloo, ON N2L 2Y5, Canada*

³*Institute for Quantum Computing, University of Waterloo, Waterloo, ON N2L 3G1, Canada*

(Dated: April 22, 2022)

We analyze the tidal deformability of a clump of dark matter particles, modelled by the collisionless Boltzmann equation. We adopt a wave-mechanical approach to the problem, in which the dynamical equations are approximated by a set of Schrödinger-Poisson equations, within the limit that the effective de Broglie wavelength is comparable to the spatial variation scale of the particle distribution. We argue that such a treatment allows for a smaller number of coupled differential equations and more accessible perturbative analyses, while keeping the description within the dynamical timescale relatively accurate. Moreover, it provides an approximate mapping between perturbed boson star configurations and dynamical dark matter clumps. We present an analysis of the tidal deformability of a minimally-coupled boson star to illustrate this (approximate) correspondence.

I. INTRODUCTION

Dark matter (DM) accounts for approximately 83% of all matter within the universe, yet its origin remains one of the most important puzzles in cosmology and physics. Among the most popular DM candidates are Weakly-Interacting-Massive-Particles (WIMPs), which only interact with each other via weak force and gravity. These WIMPs could annihilate and/or decay into other Standard Model particles and emit gamma-rays, providing indirect evidence for their existence. The annihilation cross section is expected to be $\langle\sigma v\rangle\sim 3\times 10^{-26}\text{cm}^3\text{s}^{-1}$ by matching the relic abundance after freeze-out to observations [1], and it can be constrained or measured by searches for galaxy gamma-ray excess, neutrinos experiments and cosmic rays [2]. For example, recent measurements from the Fermi Large Area Telescope (targeting dwarf spheroidal satellite galaxies of the Milky Way) [3] set a new upper-bound to this cross-section. On the other hand, for many purposes it is a good approximation to model DM dynamics (and WIMPs in particular) as collisionless particles within the cosmological timescale.

Determining the evolution of these cold DM particles requires solving a six-dimensional Boltzmann equation. This imposes real challenges for systems with large separation of scales in various physical dimensions. In order to model cosmological DM evolution and address the galaxy formation problem, modern N-body simulations [4] have been using more than 10^{10} particles, with each particle carrying $\mathcal{O}(10^8)M_\odot$ in mass. These simulations are thought to produce a reasonable description beyond certain cut-off scales, although they still raise debates such as the cuspy halo problem [5], the missing satellites problem [6], etc. On the other hand, many alternative DM candidates have been proposed, including axions [7], self-interacting dark matter [8], sterile neutrinos [9], dark waves which form a Bose-Einstein condensate [10], etc. In particular, it is possible to resolve some of the aforementioned difficulties of the cold DM model in certain alternative DM scenarios. For example, it has been sug-

gested that a coherent dark wave simulation reproduces similar signatures as N-body simulations in large scales [10], while the halo core naturally avoids the cuspy density problem, thanks to the quantum uncertainty principle that takes over at small scales.

In this work, we focus on the dynamical properties of dark matter clumps (DMCs) [11] immersed in a tidal environment. Such dense DM objects are possibly originated from primordial adiabatic isocurvature fluctuations [12], cosmological phase transitions [13], topological defects [14], accretion on primordial black holes [15], etc. However, the mass, density and radius spectra of DMCs are still highly uncertain. The ones with larger density are likely to survive from tidal interactions with the galactic environment. Depending on their mass and density, they could form binaries with stars or other dense DMCs within the globular cluster (via three body interaction or dynamical scattering), they could be captured by other star binaries, and they may pass the vicinity of supermassive black holes and give rise to tidal disruption events (TDE) [16]. In addition to the gamma rays coming from DM annihilation within these DMCs, these DMC systems and TDEs could also generate gravitational waves, with frequency lying in the band of advanced ground-based interferometers [17] and/or future space-based interferometers [18]. With recent direct detection of gravitational waves by Advanced LIGO [19] and successful launch of eLISA Pathfinder [20], it is now a good time to examine the possibility of using gravitational wave measurements to study DM physics. Understanding dynamical properties of these DMCs under gravity is therefore crucial to study the evolution of these DMC systems, to constrain their populations and to connect with observations.

A. Methodology

A useful approximation scheme for describing the dynamics of DMCs is possible when the velocity dispersion of DM particles is much smaller than the local averaged

velocity itself: in that case, the dynamics of DMCs can be approximated by a fluid with locally defined density and velocity distributions [21, 22]. However, such single-fluid description does not capture multi-streaming effects (since the velocity field is required to be single-valued) and is obviously incapable of describing more violent processes such as collisions between two DMCs. On the other hand, if the fluid approximation is valid for certain cold dark matter clumps (CDMCs), one could take advantage of it in order to examine their response to an external tidal field. The applicability of this approach is reduced, however, when one considers CDMCs under dynamical evolution. In this case, it is in principle possible to evaluate their tidal deformability in a time-averaged manner, as long as the timescale for the variation of the tidal field (T_t) is much longer than the dynamical timescale (T_d) of the CDMC. In other words, it is more convenient to study the response of ($T_d \ll \tau \ll T_t$)

$$\tilde{P}(t, \mathbf{x}, \mathbf{p}) = \frac{1}{\tau} \int_{t-\tau/2}^{t+\tau/2} dt' P(t', \mathbf{x}, \mathbf{p}),$$

under the influence of an external tidal field, where P is the phase-space distribution function satisfying the collisionless Boltzmann equation. Notice that here \tilde{P} is quasi-stationary but, more importantly, it generally no longer satisfies the fluid approximation, even if P does.

As an alternative to N -body simulations and the fluid description, Widrow and Kaiser [23] proposed to use the coupled Schrödinger-Poisson equations, together with the Husimi phase-space representation of quantum states, to obtain an approximate evolution scheme for the phase-space density distribution. Such method has also been extended by Schaller *et al.* [24], who employed the Wigner function to construct an approximate phase-space distribution. The basic idea is similar in both cases: to sample a wave function (or a set thereof) from a given phase-space distribution, evolve it according to the Schrödinger-Poisson equations and finally recover a phase-space description of the system (either through the Wigner or Husimi quasiprobability distributions). This procedure was validated against N -body simulations in [23, 25] and was shown to have comparable or reduced computational cost.

Here we shall adopt such approximate dual wave description in the investigation of the tidal deformability of DMCs, since it provides an appealing framework for perturbative analyses. In particular, we also use the Wigner function representation, as discussed in [24]. Our construction differs from [23–25] in that these approaches usually take the limit that the effective particle de Broglie wavelength is much smaller than the spatial variation scale of the particle distribution. This is done in order to accurately reproduce the distribution in position and momentum (over some cut-off scales). However, such construction is not ideal for perturbative analyses, because (i) the reconstructed distribution function has high (spatial) frequency variations, and/or (ii) there is a large number of coupled wave equations. Therefore, here we

take the limit that the effective particle de Broglie wavelength is comparable to the spatial variation scale of the particle distribution. In this way, the evolution following the Schrödinger equation in general reproduces less accurately the one following the collisionless Boltzmann equation, but we argue that the deviation mainly affects the part of phase space with small momentum. Consequently the density distribution is less affected, especially within the dynamical timescale of the system.

Within this limit, in some cases (such as for Gaussian states) it is possible to have a much simpler wave function reconstruction, which requires lower cost in numerical evolutions and is more suitable for analytical and perturbative analyses. In fact, it will be natural to see that such wave description allows an approximate mapping between well-studied boson star systems [26–28] and collisionless DMCs. In particular, in this work we compute the tidal deformability of spherical boson stars and subsequently map the result to a collisionless DMC system (with the same initial phase-space density distribution) to describe its dynamical response under an external gravitational field. To the best of our knowledge, this is the first time that concepts like tidal Love numbers have been introduced to describe dynamical properties of collisionless DM clumps. Following a similar strategy, we comment on the mapping of previous results on quasinormal modes of boson stars [29, 30] to the quasinormal modes of collisionless DMCs.

B. Structure of the paper

The organization of this paper is as follows. In Sec. II we revisit the formalism developed in [23, 24], and stress the modifications we make to facilitate perturbative analyses later on. In Sec. III a numerical demonstration is performed (one spatial dimension and one momentum dimension), for two systems with identical initial states and following respectively the Moyal and the Boltzmann equations, assuming there is a background quadratic (tidal) potential and an artificial self-gravity potential. The mass distribution density functions are compared at late times, where we find excellent agreement within the gravitational dynamical timescale. In Sec. IV we compute the $l = 2$ tidal Love number of minimally coupled boson stars, and use it to infer the Love number of the corresponding collisionless DMC. We conclude in Sec. V. Throughout most of the paper, we adopt natural units such that $c = G = 1$, but recover c 's and G 's at certain points for the sake of clarity.

II. FORMALISM

In this section, we review the relevant aspects of the formalism developed in [23], using the Wigner function representation [24]. To reduce the error in approximating the Boltzmann equation evolution, it is better to use

short-wavelength wave functions as basis for expanding the phase-space density distribution. Here we focus on another possibility, where the effective de Broglie wavelength is comparable with the spatial variation scale of the particle distribution. In this approximation scheme, we argue that, for a generic smooth gravitational potential, the mismatch in the evolution equation does not lead to large errors in the density distribution within the dynamical timescale. Moreover, such formulation allows a simpler system of evolution equations, and it is crucial for the mapping to boson star solutions used in Sec. IV.

A. Phase-space density

We consider a collisionless DM clump with total mass M and particle mass m , which is taken to be a free parameter. We denote the phase-space density distribution as $P(\mathbf{x}, \mathbf{p})$, and the collisionless Boltzmann (or Vlasov) equation can be written as

$$\frac{\partial P}{\partial t} + \frac{\mathbf{p}}{m} \cdot \nabla_{\mathbf{x}} P - m \nabla_{\mathbf{x}} U \cdot \nabla_{\mathbf{p}} P = 0, \quad (1)$$

where the gravitational potential $U(\mathbf{x})$ must satisfy the Newtonian Poisson equation

$$\nabla_{\mathbf{x}}^2 U = 4\pi m \int d^3 \mathbf{p} P(\mathbf{x}, \mathbf{p}). \quad (2)$$

In addition, the phase-space density should be normalized with respect to the total particle number

$$\int d^3 \mathbf{x} \int d^3 \mathbf{p} P(\mathbf{x}, \mathbf{p}) = \frac{M}{m}. \quad (3)$$

As long as the particle number is conserved, the concepts of phase-space density and probability density of a single particle are interchangeable, as they are proportional to each other. In other words, the phase-space density can be viewed as a probability density with total probability M/m . We shall not try to distinguish them in later analyses. The same considerations also apply for the Wigner function discussion in the next section, where we implicitly expand its definition to be the incoherent summation of the Wigner functions of M/m particles. This effective quantity is able to describe all averaged (over M/m particles) statistics of the system, and this is possible because entanglement cannot be generated through gravitational interaction between different particles in Schrödinger-Newton models [31].

B. Wigner function

Let us now recall the Wigner function for a quantum mechanical system. For simplicity, we use the notation as in 1-D systems, but it is straightforward to generalize the

discussion to higher dimensions. The Wigner function is usually defined as [32]

$$W(x, p) := \int \frac{1}{\pi \hbar} \langle x + y | \hat{\rho} | x - y \rangle e^{-2ipy/\hbar} dy, \quad (4)$$

where $\hat{\rho}$ is the density matrix for the quantum system. Correspondingly,

$$\rho(x_1, x_2) = \int W\left(\frac{x_1 + x_2}{2}, p\right) e^{-ip(x_2 - x_1)/\hbar} dp, \quad (5)$$

where $\rho(x_1, x_2) := \langle x_1 | \hat{\rho} | x_2 \rangle$. For any density matrix $\hat{\rho}$, there are always ways to decompose it into a convex combination of pure states (for example, using the Schmidt decomposition):

$$\hat{\rho} = \sum_i p_i |\psi_i\rangle \langle \psi_i|, \quad (6)$$

with $\sum_i p_i = 1$, and $p_i \geq 0$. This decomposition is not unique, which means one has the freedom to choose the state basis $\{|\psi_i\rangle\}$ to minimize the complexity (such as the number of states) in the summation. In [24], several methods are proposed to carry out such decomposition. In Sec. IIB 1 below, we present yet another method to make the expansion in Eq. (6).

The Wigner function $W(x, p)$ satisfies many properties similar to the phase-space probability distribution $P(x, p)$. For example, by integrating out one of the variables (x or p), it becomes the marginal probability distribution for the other variable. The main differences are that (i) the Wigner function can be negative (hence it is referred to as a *quasiprobability* distribution), (ii) it obeys a different evolution equation than the classical Boltzmann equation. We describe the dynamics governing the Wigner function in Sec. IIB 2 below.

1. Decomposition using coherent states

We recall the \mathcal{P} -representation of a quantum state, which is related to the density matrix by

$$\hat{\rho} = \int d^2 \alpha \mathcal{P}(\alpha) |\alpha\rangle \langle \alpha|, \quad (7)$$

where $|\alpha\rangle$ denotes a coherent state centred at α . The \mathcal{P} function $\mathcal{P}(\alpha)$ is real, and it satisfies

$$\int d^2 \alpha \mathcal{P}(\alpha) = 1. \quad (8)$$

Therefore, the \mathcal{P} function plays a role similar to p_i in Eq. (6). In fact, for the purpose of this work, it is reasonable to relax the requirement of p_i being a positive number, since the quantum formalism will be used as a mathematical tool, but no truly quantum interpretation will be sought.

The relation between the Wigner function and the \mathcal{P} function is [33]

$$W(\alpha) = \frac{2}{\pi} \int P(\gamma) e^{-2|\alpha-\gamma|^2} d^2\gamma, \quad (9)$$

and the inverse transformation is

$$\mathcal{P}(\alpha) = \exp \left[-\frac{1}{2} \frac{\partial^2}{\partial \alpha \partial \alpha^*} \right] W(\alpha), \quad (10)$$

which is uniquely determined by the Wigner function. Note that α is related to x, p by

$$\alpha = \frac{x}{\Delta_x} + i \frac{p}{\Delta_p}, \quad (11)$$

where Δ_x, Δ_p are free constants that ensure that α is dimensionless. As an example, if $W(x, p)$ is given by

$$W(x, p) = \frac{1}{\sqrt{2\pi}\sigma_x} \frac{1}{\sqrt{2\pi}\sigma_p} \exp \left[-\frac{x^2}{2\sigma_x^2} - \frac{p^2}{2\sigma_p^2} \right], \quad (12)$$

it is convenient to choose $\Delta_x = 2\sigma_x$, $\Delta_p = 2\sigma_p$, such that $W \propto e^{-2\alpha\alpha^*}$ and $\mathcal{P}(\alpha) = \delta(\alpha)\delta(\alpha^*)$.

2. Evolution equation

The time evolution of the Wigner function is governed by the Moyal equation:

$$\frac{\partial W(x, p)}{\partial t} + \{W(x, p), \hat{H}(x, p)\} = 0, \quad (13)$$

where \hat{H} is the Hamiltonian and $\{, \}$ is called Moyal bracket:

$$\{f, g\} := \frac{2}{\hbar} f(x, p) \sin \left[\frac{\hbar}{2} (\overleftarrow{\partial}_x \overrightarrow{\partial}_p - \overleftarrow{\partial}_p \overrightarrow{\partial}_x) \right] g(x, p). \quad (14)$$

Here $\overleftarrow{\partial}$ denotes the derivative operator acting on the terms to its left, and similarly for $\overrightarrow{\partial}$. In particular, if the potential is quadratic in x (e.g., tidal field): $U \propto x^2$, the Moyal equation reduces to

$$\partial_t W + \frac{p}{m} \partial_x W - m \partial_x U \partial_p W = 0, \quad (15)$$

which is precisely the collisionless Boltzmann equation. In general, after Taylor-expanding the sinusoidal operator, the Moyal evolution equation can be written as

$$\partial_t W + \frac{p}{m} \partial_x W - m \partial_x U \partial_p W + m \sum_{n=1}^{\infty} \frac{\hbar^{2n}}{(2n+1)!(2i)^{2n}} \partial_p^{2n+1} W \cdot \partial_x^{2n+1} U = 0. \quad (16)$$

Note that, by taking the $\hbar \rightarrow 0$ limit, it is possible to minimize the contributions from the terms in the second line, as long as W is sufficiently well-behaved in this limit.

From Eqs. (5) and (13), it is straightforward to derive the master equation for the density matrix $\rho(x_1, x_2)$:

$$\frac{\partial \rho}{\partial t} + \frac{i}{\hbar} \left[m[U(x_2) - U(x_1)]\rho - \frac{\hbar^2}{2m} \left(\frac{\partial^2 \rho}{\partial x_2^2} - \frac{\partial^2 \rho}{\partial x_1^2} \right) \right] = 0. \quad (17)$$

Moreover, if $U(x)$ is the gravitational potential generated by the system itself, it satisfies

$$\nabla_x^2 U = 4\pi m \rho(x, x). \quad (18)$$

Alternatively, with the decomposition given in Eq. (6), the master equation (17) can also be written as a set of coupled Schrödinger-Poisson equations,

$$i\hbar \partial_t \psi_i + \frac{\hbar^2}{2m} \nabla_x^2 \psi_i + mU \psi_i = 0, \quad (19a)$$

$$\nabla_x^2 U = 4\pi M \sum_i p_i |\psi_i|^2, \quad (19b)$$

where $\psi_i(x) := \langle x | \psi_i \rangle$ and we have modified the Poisson equation on the second line so as to adopt the standard normalization [recall the discussion below Eq. (3)]

$$\int dx |\psi_i|^2 = 1. \quad (20)$$

Finally, Eqs. (19) can be obtained as the Newtonian limit of the Einstein-Klein-Gordon equations for a collection of minimally-coupled scalar fields, which stem from the action

$$S = \int d^4x \sqrt{-g} \left[\frac{R}{16\pi} - \sum_i \left(p_i |\nabla \phi_i|^2 + p_i \frac{m^2}{\hbar^2} |\phi_i|^2 \right) \right]. \quad (21)$$

This limit, which relies on the identification $\psi_i = \phi_i e^{imt/\hbar}$ to remove the high-frequency oscillations, is discussed in more detail in Sec. IV C and is standard in quantum mechanics (for example, see [34]).

C. A wave description of collisionless DM

The coupled Schrödinger-Poisson equations (19) enable a wave description of the quantum system. In particular, they have been applied to describe the quantum state evolution of an object under a model of semi-classical gravity [35], in the case that the state is pure. They have also been used to describe scalar-wave DM candidates, and applied in cosmological simulations [10].

The applicability of the Schrödinger-Poisson equations also extends to collisionless DM models [23–25, 36]. We describe the basic idea in the following, illustrating the principles using a system with one spatial and one momentum dimension, as in Sec. II B. It is straightforward to generalize to higher dimensions.

Given an initial phase-space density distribution $P(x, p)$, which we identify with the Wigner function, we

define an effective density matrix $\sigma(x_1, x_2)$ in analogy with Eq. (5):

$$\sigma(x_1, x_2) = \int P\left(\frac{x_1 + x_2}{2}, p\right) e^{-ip(x_2 - x_1)/\varpi} dp \quad (22)$$

and, conversely,

$$P(x, p) = \int \frac{1}{\pi\varpi} \sigma(x + y, x - y) e^{-2ipy/\varpi} dy, \quad (23)$$

where ϖ is a yet undetermined constant that plays the role of \hbar in Eq. (5). The next step is to find a representation of $\sigma(x_1, x_2)$ in terms of a set of wave functions $\{\psi_i(x)\}$ [cf. Eq. (6)]; for instance, as described in Sec. II B 1. Then, the time evolution of these wave functions can be performed through the Schrödinger-Poisson equations (19). Finally, one recovers a phase-space description by applying the inverse mapping (23). In [23, 25], the Husimi quasiprobability distribution was used instead of the Wigner function as a phase-space representation of the wave functions, but the underlying idea is the same. By following this method, we trade solving the Boltzmann equation for $P(\mathbf{x}, \mathbf{p})$, which in general is six-dimensional, by solving three-dimensional coupled Schrödinger-Poisson equations for a set of complex wave functions $\psi_i(\mathbf{x})$. This is clearly computationally advantageous if the set of wave functions is not too large.

If we are to follow this procedure, there are two issues that need to be clarified. First, we need to appropriately specify the quantity ϖ that plays the role of \hbar in Eq. (22), such that the effective density matrix σ has a simple wave decomposition as in Eq. (6). Second, we need to clarify the systematic error introduced by using the Moyal equation, instead of the Boltzmann equation, to evolve P . We shall discuss the identification problem first.

1. Identification

In general, $\sigma(x_1, x_2)$, as given in Eq. (22), describes a “mixed state” and can have multiple decompositions as in Eq. (6). As an example, consider the case where P is initially Gaussian,

$$P(x, p) = \frac{1}{\sqrt{2\pi\sigma_x}} \frac{1}{\sqrt{2\pi\sigma_p}} \exp\left[-\frac{x^2}{2\sigma_x^2} - \frac{p^2}{2\sigma_p^2}\right], \quad (24)$$

where σ_x and σ_p are the variances in the position and momentum distributions, respectively. By Eq. (22), the corresponding effective density matrix is

$$\sigma(x_1, x_2) = \frac{1}{\sqrt{2\pi\sigma_x}} \exp\left[-\frac{(x_1 + x_2)^2}{8\sigma_x^2} - \frac{(x_1 - x_2)^2\sigma_p^2}{2\varpi^2}\right].$$

In order to decompose $\sigma(x_1, x_2)$ as in Eq. (6), one needs to specify the value of ϖ , that here plays the role of \hbar . In the example above, a particularly simple decomposition

ensues if one sets $\varpi = 2\sigma_x\sigma_p$. In this case, the density matrix describes a pure state: $\sigma(x_1, x_2) = \psi(x_1)\psi^*(x_2)$, where

$$\psi(x) = \left(\frac{1}{\sqrt{2\pi\sigma_x}}\right)^{1/2} \exp\left[-\frac{x^2}{4\sigma_x^2}\right].$$

Therefore, when ϖ is chosen to be $\sim \sigma_x\sigma_p$, the wave function decomposition often can be considerably simplified, e.g., for P functions that are approximately Gaussian as above, or reconstructable using the boson star configurations discussed in Sec. IV. This comes at the expense of losing the freedom to choose ϖ small and thereby minimize the error terms in the evolution equation (16). On the other hand, if ϖ is chosen to be $\ll \sigma_x\sigma_p$ as in [23, 24], the error in the evolution equation would usually be smaller, but many short-wavelength wave functions would then be needed to properly reconstruct σ . In general, the choice of ϖ depends on the accuracy required in a given problem or timescale, and the available state decomposition of a particular P .

As mentioned before, in this paper we shall focus on the case where the particle de Broglie wavelength $\lambda_{\text{deB}} := \varpi/mv$ (with $v \sim |\nabla\psi/(\partial\psi/\partial t)|$) is comparable to the spatial variation scale of the phase-space distribution ($\varpi \sim \sigma_x\sigma_p$ in the example above). In this case, we may achieve lower accuracy in describing the system’s evolution, so it would be better if the disagreement with the exact evolution was small within dynamical timescales. Let us now turn to this point.

2. Validation

With the mappings (22) and (23) between the phase-space density P and the effective density matrix σ , we can discuss the error involved in using the wave approximation above, in terms of evolution equations for σ . On the one hand, as P must follow the collisionless Boltzmann equation (1), consequently σ must follow

$$\begin{aligned} \frac{\partial\sigma}{\partial t} + \frac{i}{\varpi} \left[m(x_2 - x_1) \cdot \nabla U \left(\frac{x_1 + x_2}{2} \right) \sigma \right. \\ \left. - \frac{\varpi^2}{2m} \left(\frac{\partial^2\sigma}{\partial x_2^2} - \frac{\partial^2\sigma}{\partial x_1^2} \right) \right] = 0. \end{aligned} \quad (25)$$

On the other hand, by using the wave approximation above, we are effectively evolving σ using the master equation [cf. Eq. (17)]

$$\frac{\partial\sigma}{\partial t} + \frac{i}{\varpi} \left[m[U(x_2) - U(x_1)]\sigma - \frac{\varpi^2}{2m} \left(\frac{\partial^2\sigma}{\partial x_2^2} - \frac{\partial^2\sigma}{\partial x_1^2} \right) \right] = 0. \quad (26)$$

Comparing Eqs. (25) and (26), we find that the only difference is the potential related term, where the $(x_2 - x_1) \cdot \nabla U$ term in Eq. (25) can be viewed as a first order Taylor expansion of $U(x_2) - U(x_1)$, in Eq. (26), around the middle point $(x_2 + x_1)/2$. If the potential is linear

or quadratic in x , which is the case for tidal fields, such difference vanishes and the two equations are identical. In general, the higher-order terms in the Taylor expansion will cause systematic errors when we use Eq. (26) to evolve the system. Obviously the error should be smaller for near-diagonal terms in the density matrix, where $|x_1 - x_2|$ is small. In fact, when we take the $\varpi \rightarrow 0$ limit, we see from Eq. (22) that the effective density matrix σ associated with a given P becomes increasingly diagonal: the integral is non-negligible only when $x_1 \approx x_2$, due to the rapid phase oscillations in the integrand otherwise. Thus, the influence of error terms becomes less important in this regime, in agreement with our previous discussion. Nevertheless, if we are mainly interested in the evolution of the spatial mass distribution $\sigma(x, x)$, Eq. (26) actually provides a reasonable description within the gravitational dynamical timescale, even not in the $\varpi \rightarrow 0$ limit, as we illustrate later using a numerical simulation.

The inaccurate far-off-diagonal components in σ mainly affect the low-momentum part of the phase space when we use Eq. (23) to reconstruct the phase-space distribution, as the $e^{2ipy/\varpi}$ factor becomes highly oscillatory when the magnitude of p, y is large. This is consistent with the observation that the mass distribution is less affected by the systematic error, as the change of mass density in short timescales is more vulnerable to “fast” particles. On the other hand, the P function obtained from evolving σ according to Eq. (26) is essentially the Wigner function of Sec. II B, which may become negative at part of the phase space during evolution. In fact, in most cases the negative value region is mainly located at the “low-momentum” part of the phase space. Again, an accurate description of the mass distribution already reveals a lot of information about the system, especially its gravitational properties.

3. Consistency check: tidal disruption without self-gravity

In [16], a DMC under a strong tidal gravitational field was analyzed (see also [37]). In particular, the self-gravity produced by the DMC was neglected and the motion of DM particles in each direction was treated as independent. As shown in [16] and [37], given the initial phase-space density, its later distribution can be obtained by applying the conservation of phase-space density implied by Liouville’s theorem and solving for the trajectory of each DM particle. We shall use this example to illustrate how to apply the effective wave description to derive later distributions. As the potential here is purely quadratic, the effective approach should produce the same result as the one by the Boltzmann equation (or Liouville’s theorem). As the motion of particles is independent in the x, y, z directions, we can simplify the problem to 1-D, and take $U_{\text{tide}} = \alpha x^2$ ($\alpha > 0$, the case with $\alpha < 0$ can be analyzed similarly).

Similarly to [16], we assume a Gaussian initial distri-

bution, as given in Eq. (24). Correspondingly, we can choose

$$\psi(t=0, x) = \left(\frac{1}{\sqrt{2\pi}\sigma_x} \right)^{1/2} e^{-\frac{x^2}{4\sigma_x^2}}, \quad (27)$$

and $\varpi = 2\sigma_x\sigma_p$. It is straightforward to check that the “Wigner function” of this wave function reproduces the initial phase-space density in Eq. (24). The Schrödinger equation we need to solve is

$$i\varpi \frac{\partial \psi}{\partial t} + \frac{\varpi^2}{2m} \nabla_x^2 \psi - m\alpha x^2 \psi = 0. \quad (28)$$

Instead of trying to solve for $\psi(t)$ directly, we notice that a Gaussian wave packet remains Gaussian under a quadratic potential, which means we only need to know its mean and variance to determine its shape. To obtain mean and variance, we adopt the Heisenberg picture:

$$\dot{\hat{x}} = \frac{\hat{p}}{m}, \quad \dot{\hat{p}} = -2m\alpha \hat{x}. \quad (29)$$

These equations have the following solution in terms of \hat{x}_0, \hat{p}_0 :

$$\hat{x} = \hat{x}_0 \cos \omega t + \frac{\hat{p}_0}{m\omega} \sin \omega t, \quad \hat{p} = \hat{p}_0 \cos \omega t - \omega m \hat{x}_0 \sin \omega t, \quad (30)$$

with $\omega^2 = 2\alpha$. Therefore the variance at time t is just

$$\begin{aligned} \text{Var}[\hat{x}] &= \langle \hat{x}^2 \rangle = \text{Var}[\hat{x}_0] \cos^2 \omega t + \frac{\text{Var}[\hat{p}_0]}{m^2 \omega^2} \sin^2 \omega t \\ &= \sigma_x^2 \cos^2 \omega t + \frac{\sigma_p^2}{m^2 \omega^2} \sin^2 \omega t, \\ \text{Var}[\hat{p}] &= \langle \hat{p}^2 \rangle = \sigma_p^2 \cos^2 \omega t + m^2 \omega^2 \sigma_x^2 \sin^2 \omega t, \\ \text{Cov}[\hat{x}\hat{p}] &= \frac{1}{2} \langle \hat{x}\hat{p} + \hat{p}\hat{x} \rangle = \frac{\sin 2\omega t}{2} \left(\frac{\sigma_p^2}{m\omega} - m\omega \sigma_x^2 \right), \end{aligned}$$

where we have used the fact that $\langle \hat{x}_0 \hat{p}_0 \rangle = 0$. With these variances we can easily reconstruct the corresponding Wigner function, as it must retain Gaussian shape. We can check then it is consistent with the calculation using Liouville’s theorem in phase space in [16]. In fact, if we use Liouville’s theorem and write down the equations of motion in phase space, they are just the “classical” version of the Heisenberg equations of motion in Eq. (29). In this sense, the equivalence of the two approaches is rather natural.

III. NUMERICAL COMPARISON IN A 1-D PROBLEM

In this section, we compare the evolution of the effective density matrix $\sigma(x_1, x_2)$ according to Eq. (25) and Eq. (26), which are associated to the collisionless Boltzmann equation and the Moyal equation, respectively. As

we saw in the previous section, in the approximation of no self-gravity, a DMC in a tidal environment can be described by either of these equations with identical results. A natural question that follows is whether an approximate agreement is maintained when self-gravity is taken into account. In this section we address this question. However, in order to avoid the complications introduced by having to solve self-consistently for the gravitational potential, we assume instead an artificial attractive potential in addition to the tidal field; namely

$$U(x) = \alpha_1 x^2 - \alpha_2 e^{-x^2/a^2}. \quad (31)$$

Throughout this Section c 's and G 's will be conveniently restored. The constant α_1 scales as $\alpha_1 \sim GM'/R'^3$, where M' is the mass of a second body, responsible for generating the tidal field, and R' is the distance of the DMC to it. The constant α_2 scales as $\alpha_2 \sim GM/R$, where M and R are the mass and radius of the DMC. Naturally, $a \sim R$. The contributions of the two terms in Eq. (31) are comparable if R' is of the order of the *tidal radius*, defined as $R_t = (M'/M)^{1/3}R$.

It is convenient to define the dimensionless quantities

$$\tilde{t} := t \frac{mc^2}{\varpi}, \quad \tilde{x} := x \frac{mc}{\varpi}, \quad \tilde{U} := \frac{U}{c^2}. \quad (32)$$

In terms of them Eqs. (25) and (26) assume the following forms:

$$\frac{1}{i} \frac{\partial \sigma}{\partial \tilde{t}} + (\tilde{x}_2 - \tilde{x}_1) \cdot \nabla \tilde{U} \left(\frac{\tilde{x}_1 + \tilde{x}_2}{2} \right) \sigma - \frac{1}{2} \left(\frac{\partial^2 \sigma}{\partial \tilde{x}_2^2} - \frac{\partial^2 \sigma}{\partial \tilde{x}_1^2} \right) = 0 \quad (33)$$

and

$$\frac{1}{i} \frac{\partial \sigma}{\partial \tilde{t}} + [\tilde{U}(\tilde{x}_2) - \tilde{U}(\tilde{x}_1)] \sigma - \frac{1}{2} \left(\frac{\partial^2 \sigma}{\partial \tilde{x}_2^2} - \frac{\partial^2 \sigma}{\partial \tilde{x}_1^2} \right) = 0. \quad (34)$$

At $t = 0$, we specify Gaussian initial data for the effective density matrix σ ,

$$\sigma(t = 0; \tilde{x}_1, \tilde{x}_2) = \frac{1}{\sqrt{2\pi\sigma_x}} e^{-(\tilde{x}_1^2 + \tilde{x}_2^2)/(4\sigma_x^2)}. \quad (35)$$

As we saw in Sec. IIC1, this is the density matrix obtained from a Gaussian phase-space density distribution P in the limit where the particle de Broglie wavelength is comparable to the variation scale of the particle distribution (i.e. $\varpi \sim \sigma_x \sigma_p$). We then let the initial data (35) evolve according to Eq. (33) and Eq. (34), and compare the respective outcomes $\sigma_{\text{exact}}(t; x_1, x_2)$ and $\sigma_{\text{approx}}(t; x_1, x_2)$ at later times.

For the results presented below, we set $\sigma_x = 5$, $\alpha_1 = 10^{-4}(mc^2/\varpi)^2$, $\alpha_2 = 0.5c^2$, and $a = 10\varpi/mc$. From the scaling considerations below Eq. (31), we can see that $R' \sim 3.7R_t$ for this choice of parameters. Also, it is useful to define $T := \sqrt{R^3/GM}$, which gives the dynamical timescale of the DMC. Defining a dimensionless timescale as in Eq. (32), we find that $\tilde{T} := Tmc^2/\varpi \approx 15$ for the parameters above.

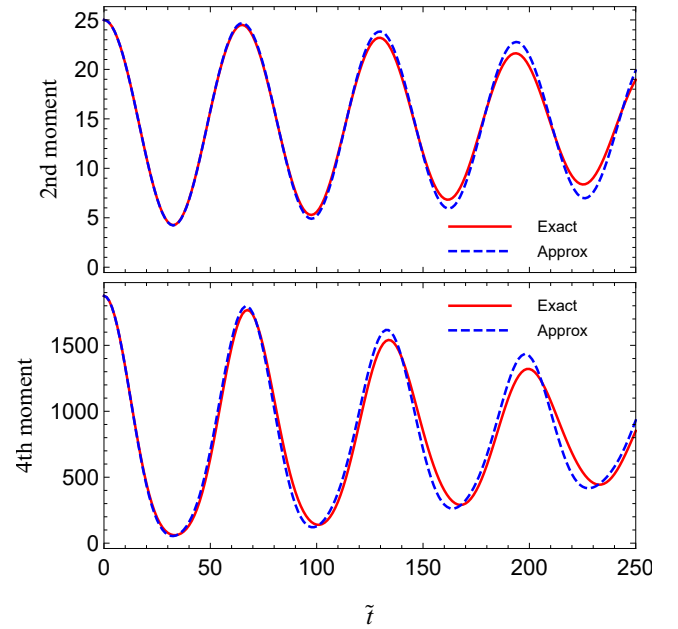


FIG. 1: Second and fourth moments of the density distributions $\sigma_{\text{exact}}(x, x)$ and $\sigma_{\text{approx}}(x, x)$ as functions of time.

The numerical setup is the following. We discretize Eqs. (33) and (34) in a uniform grid with n^2 nodes $(\tilde{x}_{1,i}, \tilde{x}_{2,j}) = (-L/2 + i\Delta x, -L/2 + j\Delta x)$, where $i, j \in \{0, 1, \dots, n-1\}$, $\Delta x := L/(n-1)$, and L determines the size of the numerical domain. For the results presented here, we take $L = 200$ and $n = 401$. The space derivatives are discretized with central finite differences and we evolve in time using a fourth-order Runge-Kutta algorithm. The time step is given by $\Delta t = \kappa(\Delta x)^2$, with $\kappa = 0.25$.

For many applications (such as computing the gravitational response), we are primarily interested in the density distribution $\sigma(x, x)$. In Fig 1, we show the second and fourth moments of the density distributions $\sigma_{\text{exact}}(x, x)$ and $\sigma_{\text{approx}}(x, x)$, as functions of time. We see that the distributions are very close to each other within the dynamical timescale, and that they follow a similar evolution for an even longer period of time. In Fig. 2, we show the (normalized) trace distance between the “density matrices” $\sigma_{\text{exact}}(x_1, x_2)$ and $\sigma_{\text{approx}}(x_1, x_2)$, and the total variation distance between the distributions $\sigma_{\text{exact}}(x, x)$ and $\sigma_{\text{approx}}(x, x)$. The plot indicates, in agreement with our previous discussion, that these matrices differ mostly in their nondiagonal components, which generally affect the part of P with small momentum and have lower impact in the gravitational properties of the system.

Thus, we find further evidence that, even in the limit where the effective particle de Broglie wavelength is not tuned to be small, but is taken to be comparable with the size of system, the error incurred in the wave-mechanical method described here is small at least within the dynamical timescale of the system.

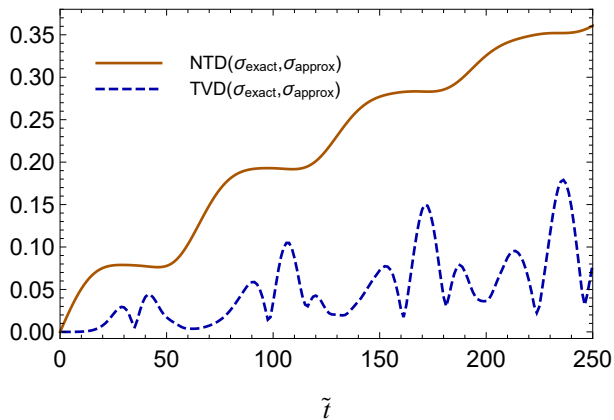


FIG. 2: Normalized trace distance and total variation distance between σ_{exact} and σ_{approx} , as a function of time. We define $\text{NTD}(\rho, \sigma) := \|\rho - \sigma\|_1 / (\|\rho\|_1 + \|\sigma\|_1)$, where $\|\rho\|_1 := \frac{1}{2} \text{Tr}[\sqrt{\rho^\dagger \rho}]$, and $\text{TVD}(\rho, \sigma) := \frac{1}{2} \sum_x |\rho(x, x) - \sigma(x, x)| \Delta x$. Note that the total variation distance is restricted to the diagonals of the matrices, which are valid probability distributions. Both distance measures lie in the interval $[0, 1]$.

IV. BOSON STARS IN A TIDAL ENVIRONMENT

In this section, we analyze the response of a boson star (see [26–28] for reviews) to an applied tidal field, and then use the mapping described subsequently to obtain similar properties for DMCs. Since the results for the tidal deformability of boson stars can be of interest on their own, here we present the full relativistic calculation, discussing later the appropriate Newtonian limit, which is probably more relevant in astrophysical scenarios. Note that the Einstein-Klein-Gordon system can also serve to approximate the dynamics of collisionless matter in general relativity [38].

We consider a massive (complex) scalar field minimally coupled to gravity and with no self-interaction, described by the action

$$S = \int d^4x \sqrt{-g} \left[\frac{R}{16\pi} - \nabla_\alpha \Phi^* \nabla^\alpha \Phi - \mu^2 |\Phi|^2 \right], \quad (36)$$

where $\mu := m/\hbar$ is a mass parameter with units of inverse length. The field equations that follow from Eq. (36) are the Einstein,

$$G_{\alpha\beta} = 8\pi \left[\nabla_\alpha \Phi^* \nabla_\beta \Phi + \nabla_\beta \Phi^* \nabla_\alpha \Phi - g_{\alpha\beta} (\nabla_\rho \Phi^* \nabla^\rho \Phi + \mu^2 |\Phi|^2) \right], \quad (37)$$

and Klein-Gordon,

$$\nabla^\alpha \nabla_\alpha \Phi = \mu^2 \Phi, \quad (38)$$

equations, together with the complex conjugate of Eq. (38). In the following, we first construct spherically symmetric equilibrium solutions of Eqs. (37) and (38) and then consider perturbations to these solutions,

sourced by an external, nearly static tidal field, characterized by the quadrupole tidal moment \mathcal{E}_{ij} . In a Newtonian setting, $\mathcal{E}_{ij} := \partial_i \partial_j U_{\text{ext}}$, where U_{ext} is the external potential (which is evaluated at the body's center of mass after differentiation) [39]. In response to the applied tidal field, the star develops a nonzero quadrupole moment Q_{ij} , which, to linear order, is proportional to \mathcal{E}_{ij} , $Q_{ij} = -\lambda \mathcal{E}_{ij}$. More specifically, in the star's local rest frame, to leading order, the metric component g_{tt} can be written as [40]

$$g_{tt} = -1 + \frac{2M}{r} - \mathcal{E}_{ij} x^i x^j \left(1 + \frac{3\lambda}{r^5} \right), \quad (39)$$

where M is the star's gravitational mass and x^i defines a Cartesian coordinate system, with $r^2 := \delta_{jk} x^j x^k$. Equation (39) includes the external quadrupolar tidal potential and the leading order response from the body. The coefficient λ gives a measure of the deformability of the boson star, and this is the quantity we ultimately want to compute.

A. Background

We choose the unperturbed configuration to be spherically symmetric and static, in which case the spacetime line element can be written as

$$ds^2 = -e^{v(r)} dt^2 + e^{u(r)} dr^2 + r^2 d\theta^2 + r^2 \sin^2 \theta d\varphi^2. \quad (40)$$

The scalar field is taken to have a harmonic time dependence,

$$\Phi_0(t, r) = e^{-i\omega t} \phi_0(r), \quad (41)$$

which is consistent with a static gravitational field. With these ansatzes, the field equations (37) and (38) reduce to the following set of ordinary differential equations:

$$u' = \frac{1 - e^u}{r} + 8\pi r e^u [(\omega^2 e^{-v} + \mu^2) \phi_0^2 + e^{-u} \phi_0'^2], \quad (42a)$$

$$v' = \frac{e^u - 1}{r} + 8\pi r e^u [(\omega^2 e^{-v} - \mu^2) \phi_0^2 + e^{-u} \phi_0'^2], \quad (42b)$$

$$\phi_0'' + \left(\frac{2}{r} + \frac{v' - u'}{2} \right) \phi_0' + e^u (\omega^2 e^{-v} - \mu^2) \phi_0 = 0, \quad (42c)$$

with a prime denoting a radial derivative. Note that it is possible to define dimensionless variables $\tilde{r} = \mu r$ and $\tilde{\omega} = \omega/\mu$, in terms of which the equations above are not explicitly μ -dependent.

Equations (42) must be solved subject to regularity conditions at $r = 0$, namely $u(0) = 0$ and $\phi_0'(0) = 0$, and boundary conditions at spatial infinity:

$$\lim_{r \rightarrow \infty} v(r) = 0, \quad \lim_{r \rightarrow \infty} \phi_0(r) = 0. \quad (43)$$

For a given value of $\phi_c := \phi_0(0)$, solutions satisfying these boundary conditions exist only for a discrete set

of eigenfrequencies ω . They are computed numerically by a shooting algorithm, which we briefly describe. We evolve the system (42) from $r = 0$, with initial conditions $u(0) = 0$, $v(0) = v_c$, $\phi_0(0) = \phi_c$, and $\phi_0'(0) = 0$, where v_c is in principle arbitrary. For a given value of $\phi_c > 0$, the solution thus obtained for $\phi_0(r)$ diverges to $+\infty$ when $\omega \approx 0$; then, as we increase the value of ω , to $-\infty$ after crossing zero once, then to $+\infty$ after crossing zero twice, and so forth. Solutions with vanishing scalar field at spatial infinity, and different number of nodes, exist for frequencies ω in the threshold between these various asymptotic behaviours. We are interested in the ground-state solution, which has no nodes. By fine-tuning the value of ω , we can obtain an approximation to this solution, which crosses zero at increasingly higher values of r . The numerical solution thus obtained is in general such that $v_\infty := \lim_{r \rightarrow \infty} v(r) \neq 0$. However, since Eqs. (42) are invariant under a constant shift in $v(r)$, $v \rightarrow v + v_0$, accompanied by a rescaling in frequency, $\omega \rightarrow e^{v_0/2}\omega$, the actual solution, satisfying the correct boundary conditions, can be obtained a posteriori by $v(r) \rightarrow v(r) - v_\infty$, $\omega \rightarrow e^{-v_\infty/2}\omega$.

By varying the central value of the scalar field, we obtain a sequence of boson star configurations, as shown in Fig. 3. In the upper panel, the frequency ω , obtained through the shooting procedure described above, is shown as a function of ϕ_c . We notice that $\omega \rightarrow \mu$ as $\phi_c \rightarrow 0$, as characteristic of the Newtonian limit. The gravitational mass of the star is defined as $M = \lim_{r \rightarrow \infty} m(r)$, where $m(r) := (r/2)(1 - e^{-u(r)})$ and is plotted in the lower panel of Fig. 3. As for fluid stars, we see a turning point in the M - ϕ_c diagram, signalling a change in stability of the equilibrium configurations. Stable configurations exist for $\phi_c \lesssim 0.054$.

Finally, note that, since the scalar field profile decays exponentially for $r \gg 1/\mu$, it is possible to define an effective notion of radius of the boson star [27]; for instance, we can define the effective radius R as being such that $m(R) = 0.99M$.

B. Perturbations

In order to determine the response of a boson star to an applied tidal field, we first consider general perturbations of the equilibrium configuration. We write

$$g_{\alpha\beta} = g_{\alpha\beta}^{(0)} + h_{\alpha\beta}, \quad \Phi = \Phi_0 + \delta\Phi, \quad (44)$$

where $g_{\alpha\beta}^{(0)}$ is given by Eq. (40) and Φ_0 is given by Eq. (41), and work in first order in the perturbed quantities. We adopt the Regge-Wheeler gauge and restrict consideration to quadrupolar ($l = 2$) even-parity static

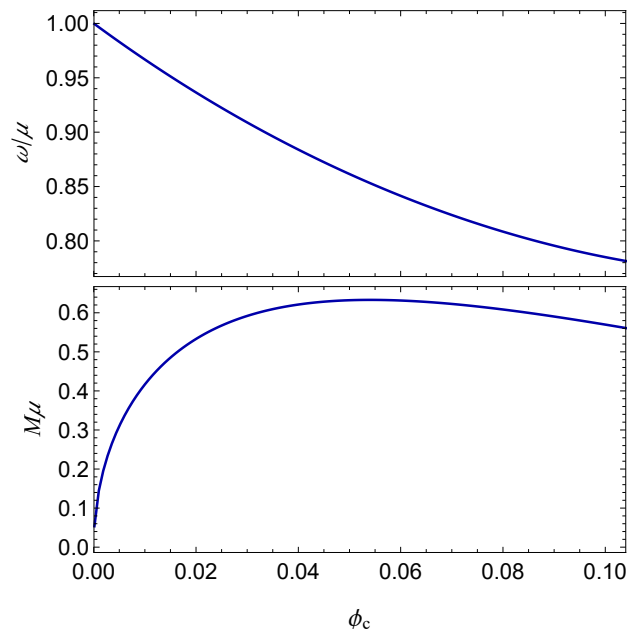


FIG. 3: Sequence of equilibrium boson star configurations, labelled by value ϕ_c of the central scalar field. The frequency ω and the total mass M are shown as a function of ϕ_c .

perturbations of the metric, namely,

$$h_{\alpha\beta} = \sum_{m=-2}^2 Y_{2m}(\theta, \varphi) \times \text{diag}[-e^{v(r)}H_0(r), e^{u(r)}H_2(r), r^2K(r), r^2\sin^2\theta K(r)]. \quad (45)$$

We further write the scalar field perturbation as

$$\delta\Phi(t, r, \theta, \varphi) = \sum_{m=-2}^2 e^{-i\omega t} \frac{\phi_1(r)}{r} Y_{2m}(\theta, \varphi). \quad (46)$$

By requiring $\delta\Phi$ to have the same time dependence as the background field, we assure that the perturbed energy-momentum tensor is static to linear order.

We then insert Eqs. (45) and (46) into the linearized Einstein's equations, $\delta G_{\alpha\beta}^{\alpha} = 8\pi\delta T_{\beta}^{\alpha}$. The $\theta\theta$ - minus the $\phi\phi$ -component reveal that $H_2(r) = -H_0(r)$. Also, the $r\theta$ -component can be used to relate K' to ϕ_1 , H_0 , and its derivative:

$$K' = -H_0' - H_0v' - \frac{32\pi\phi_1\phi_0'}{r}. \quad (47)$$

Finally, the rr - minus the tt -component can be written as a master equation for H_0 , with no further K dependence:

$$\begin{aligned} H_0''(r) + \frac{4 - ru' + rv'}{2r} H_0'(r) \\ + \left(32\pi e^{u-v}\omega^2\phi_0^2 - \frac{6e^u}{r^2} + \frac{2v'}{r} - \frac{u'v'}{2} - \frac{v'^2}{2} + v'' \right) H_0 \\ = \frac{16\pi}{r^2} [2re^{u-v}\omega^2\phi_0 - (4 - ru' - rv')\phi_0' - 2r\phi_0''] \phi_1. \end{aligned} \quad (48)$$

Additionally, the perturbed scalar wave equation reads

$$\left[\frac{d^2}{dr_*^2} + \omega^2 - e^v \left(\frac{7 - e^{-u}}{r^2} + \mu^2 - 8\pi\mu^2\phi_0^2 + 32\pi e^{-u}\phi_0'^2 \right) \right] \phi_1 = [2r\omega^2\phi_0 - e^v r (\mu^2\phi_0 - e^{-u}v'\phi_0')] H_0, \quad (49)$$

where r_* is defined through $dr_* = e^{(u-v)/2} dr$. Our task is to solve the coupled system formed by Eqs. (48) and (49) subject to suitable boundary conditions. Note that, again, it is possible to scale away the μ dependence of these equations by suitable variable redefinitions.

Around $r = 0$, the leading-order behaviour of $H_0(r)$ and $\phi_1(r)$ is given by

$$H_0(r) \approx H_0^{(2)} r^2 + O(r^4), \quad \phi_1(r) \approx \phi_1^{(3)} r^3 + O(r^5). \quad (50)$$

Since Eqs. (48) and (49) are invariant under an overall normalization of H_0 and ϕ_1 , we can fix, say, $H_0^{(2)} = 1$ and retrieve the correct normalization a posteriori (in our case, this would be determined by the strength of the tidal environment). The value of $\phi_1^{(3)}$ is determined by imposing

$$\lim_{r \rightarrow \infty} \phi_1(r) = 0. \quad (51)$$

The procedure for constructing a numerical solution is entirely analogous to what was described previously: by fine-tuning the value of $\phi_1^{(3)}$, we guarantee that condition (51) is satisfied in a sufficiently large domain. Notice from Eq. (49) that since $\phi_0(r)$ goes to zero exponentially as $r \rightarrow \infty$, the boundary condition (51) is not inconsistent with a polynomial growth for $H_0(r)$ in this limit, which is to be expected by Eq. (39).

For distances much larger than the typical size R of the boson star, Eq. (48) takes the form

$$H_0'' + H_0' \left(\frac{2}{r} + e^u \frac{2M}{r^2} \right) - H_0 \left(\frac{6e^u}{r^2} + e^{2u} \frac{4M^2}{r^4} \right) = 0, \quad (52)$$

where we used that $u' = -v' = -2Me^u/r^2$ in this regime. Equation (52) has the general solution (in terms of associate Legendre functions):

$$H_0(r) \approx c_1 Q_2^2(r/M - 1) + c_2 P_2^2(r/M - 1), \quad (53)$$

valid for $r \gg R$, and which behaves as

$$H_0(r) \approx 3 \left(\frac{r}{M} \right)^2 c_2 + O(r^3) + \frac{8}{5} \left(\frac{M}{r} \right)^3 c_1 + O(r^{-4}) \quad (54)$$

as $r \rightarrow \infty$. The growing piece of the metric perturbation accounts for the presence of an external tidal field, while the decaying piece encodes the response of the body. By matching this asymptotic form with Eq. (39), one infers that $\lambda = (8M^5/5)c_1/c_2$. Therefore, the value of λ can be inferred from the numerical solution at $r = R_{\text{ext}} \gg R$ by evaluating $y := R_{\text{ext}} H_0'(R_{\text{ext}})/H_0(R_{\text{ext}})$ and computing

[41]

$$\begin{aligned} \lambda &= \frac{16}{15} M^5 (1 - 2\mathcal{C})^2 [2 + 2\mathcal{C}(y - 1) - y] \\ &\times \{ 3(1 - 2\mathcal{C})^2 [2 - y + 2\mathcal{C}(y - 1)] \log(1 - 2\mathcal{C}) \\ &+ 2\mathcal{C}[6 - 3y + 3\mathcal{C}(5y - 8)] + 4\mathcal{C}^3 [13 - 11y \\ &+ \mathcal{C}(3y - 2) + 2\mathcal{C}^2(1 + y)] \}^{-1}, \end{aligned} \quad (55)$$

where $\mathcal{C} := M/R_{\text{ext}}$. For sufficiently large extraction radius R_{ext} , the value thus obtained for λ is independent of R_{ext} .

For fluid stars, the $l = 2$ tidal Love number is usually defined as $k_2 := (3/2)R_s^{-5}\lambda$, where R_s is the stellar radius. This is convenient not only because k_2 is a dimensionless quantity, but also because it has a meaningful Newtonian limit. Indeed, as we approach the Newtonian regime, the star becomes less compact and the stellar radius grows for a fixed mass. Since λ typically grows as R_s^5 , this definition guarantees that k_2 is finite in the limit of $R_s \rightarrow \infty$. A similar behaviour is found for boson stars as $\phi_c \rightarrow 0$ (or $M \rightarrow 0$; $R \rightarrow \infty$). In this limit, we can verify that λ grows as R^5 , as M^{-5} , or as $\phi_c^{-5/2}$. Since the usual definition of k_2 is quite sensitive to the value of the radius (as it enters to the 5th power), which is inherently ambiguous for boson stars, we choose instead to define the quantity

$$k_{\text{BS}} := \lambda M^5. \quad (56)$$

This quantity is plotted as a function of ϕ_c in Fig. 4, and has a finite limit as $\phi_c \rightarrow 0$.

In the next subsection, we shall compute independently the value of k_{BS} in the Newtonian limit. While the calculation is mostly analogous to what we did so far, it offers a few new insights and works as a consistency check of the relativistic calculation. The Newtonian value of k_{BS} is exhibited as a red open circle in Fig. 4 and is consistent with the trend of the relativistic curve.

C. Newtonian limit

In this subsection we repeat the steps of the relativistic calculation presented above, but for the Schrödinger-Poisson system, which follows as the Newtonian limit of the Einstein-Klein-Gordon equations (37)-(38). For the sake of clarity, throughout this subsection we recover the lost factors of c 's and G 's.

The Newtonian limit of the Einstein-Klein-Gordon equations can be obtained by setting (in Cartesian coordinates)

$$\begin{aligned} g_{tt} &= -c^2 [1 + 2U/c^2 + \mathcal{O}(c^{-4})] \\ g_{ij} &= (1 - 2U/c^2) \delta_{ij} + \mathcal{O}(c^{-4}). \end{aligned} \quad (57)$$

We further write $\Phi = e^{imc^2 t/\hbar} \Psi$, thereby factoring out the high-frequency oscillations of the field. To leading order (in $1/c$), Eq. (37) gives rise to the Poisson equation,

$$\nabla^2 U = 8\pi G(m/\hbar)^2 |\Psi|^2, \quad (58)$$

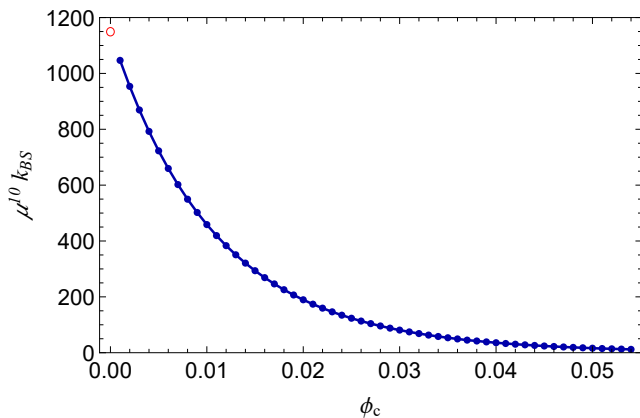


FIG. 4: For a sequence of equilibrium boson stars, characterized by the central value of the scalar field ϕ_c , we plot the tidal number $k_{\text{BS}} := \lambda M^5$, rescaled by μ^{10} to yield a dimensionless quantity. The Newtonian value, as computed in Sec. IV C, is shown as a red open circle.

while Eq. (38) reduces to the Schrödinger equation

$$i\hbar \frac{\partial \Psi}{\partial t} = -\frac{\hbar^2}{2m} \nabla^2 \Psi + mU\Psi, \quad (59)$$

where we used that $\mu := mc/\hbar$. The Newtonian analogue of a boson star is then a stationary solution of the form $\Psi(t, r) = e^{iEt/\hbar} \psi_0(r)$, which can be constructed numerically along the same lines described in Sec. IV A.

Interestingly, Eqs. (58) and (59) are invariant under the transformation

$$\Psi \rightarrow C\Psi, \quad U \rightarrow CU, \quad r \rightarrow C^{-1/2}r, \quad t \rightarrow C^{-1}t, \quad (60)$$

where C is an arbitrary constant. This implies that, contrary to the case of boson stars, in which there is a family of solutions parametrized by the central value of the scalar field, stationary solutions of the Schrödinger-Poisson equations with different values of $\psi_c = \psi_0(0)$ can be trivially related by a rescaling of the form (60). In particular, the solution's total mass, defined as $M := \lim_{r \rightarrow \infty} rU(r)/G$, transforms as $M \rightarrow C^5 M$ under a change of normalization $\Psi \rightarrow C\Psi$.

In order to determine the tidal deformability of a “Newtonian boson star”, we consider general perturbations of the form

$$U = U_0 + \delta U, \quad \Psi = \Psi_0 + \delta \Psi, \quad (61)$$

where U_0 and Ψ_0 denote a background stationary solution and we write

$$\delta U = \frac{1}{2} \sum_{m=-2}^2 e^{iEt/\hbar} H(r) Y_{2m}(\theta, \varphi),$$

$$\delta \Psi = \sum_{m=-2}^2 e^{iEt/\hbar} \frac{\psi_1(r)}{r} Y_{2m}(\theta, \varphi).$$

To linear order, the perturbation equations become

$$H'' + \frac{2}{r}H' - \frac{6H}{r^2} = \frac{16\pi Gm^2}{\hbar^2 r} (\psi_1^* \psi_0 + \psi_1 \psi_0^*) \quad (62)$$

and

$$\psi_1'' - \left[\frac{6}{r^2} + \frac{2m}{\hbar^2} (mU_0 + E) \right] \psi_1 = \frac{m^2}{\hbar^2} r H \psi_0. \quad (63)$$

Given a background solution for ψ_0 , U_0 and E , the perturbation equations can be solved numerically by a procedure entirely analogous to the one described in Sec. IV B: by adjusting the value of $\psi_1^{(3)} = \psi_1'''(0)$ one ensures that the boundary condition $\lim_{r \rightarrow \infty} \psi_1(r) = 0$ is satisfied in a sufficiently large numerical domain.

For distances much larger than the typical size R of the star, the source term in Eq. (62) vanishes and $H(r)$ behaves as

$$H(r) \approx \frac{d_1}{r^3} + d_2 r^2. \quad (64)$$

It is straightforward to infer that $\lambda = (1/3)d_1/d_2$ [see Eq. (39)]. Therefore, λ can be computed from numerical data at an extraction radius $R_{\text{ext}} \gg R$ by

$$\lambda = R_{\text{ext}}^5 \frac{2 - y}{3(3 + y)}, \quad (65)$$

where again $y := R_{\text{ext}} H'(R_{\text{ext}})/H(R_{\text{ext}})$. Equation (65) is the Newtonian limit of Eq. (55), obtained by neglecting corrections of higher order in $\mathcal{C} = GM/(c^2 R_{\text{ext}})$. Again, for sufficiently large R_{ext} , the value thus obtained for λ is independent of R_{ext} ; indeed, as $R_{\text{ext}} \rightarrow \infty$, we have that $y \rightarrow 2$ in such a way that Eq. (65) has a well-defined limit.

As discussed before, the Schrödinger-Poisson equations remain invariant under the transformation (60). However, the same is *not* true for λ , which transforms as $\lambda \rightarrow C^{-5/2} \lambda$. A more meaningful quantity is given, e.g., by $k_{\text{BS}}^{(N)} = \lambda(GM/c^2)^5$, defined in analogy with Eq. (56). This tidal number is not affected by a renormalization of the wave function and can be computed to be

$$k_{\text{BS}}^{(N)} = 1149 \times (\hbar/mc)^{10}. \quad (66)$$

As shown in Fig. 4, this value is consistent with the appropriate limit of the relativistic calculation.

D. Mapping to a DMC

With the results for the tidal Love number of boson stars, we are now in a position to discuss their implications to the perturbative behavior of DMCs. For this purpose, it is useful to rewrite the Schrödinger-Poisson equations (19) in terms of dimensionless (spatial, temporal and mass) variables, obtained through [cf. Eq. (32)]

$$t \rightarrow \left(\frac{mc^2}{\hbar}\right)^{-1} \times \tilde{t}, \quad (67a)$$

$$\mathbf{x} \rightarrow \left(\frac{mc}{\hbar}\right)^{-1} \times \tilde{\mathbf{x}}, \quad (67b)$$

$$M \rightarrow \left(\frac{\hbar c}{Gm}\right) \times \tilde{M}, \quad (67c)$$

in which case the wave equation becomes

$$i\partial_{\tilde{t}}\psi = -\frac{1}{2}\tilde{\nabla}^2\psi + \tilde{M}\psi \int d^3\tilde{\mathbf{x}}' \frac{|\psi(\tilde{\mathbf{x}}')|^2}{|\tilde{\mathbf{x}} - \tilde{\mathbf{x}}'|}, \quad (68)$$

where the wave function normalization is fixed to be

$$\int d^3\tilde{x}' |\psi(\mathbf{x}')|^2 = 1. \quad (69)$$

Equations (67) can be used to map between truly wave-mechanical systems such as boson stars and cold dark matter models. For example, a DMC with total mass M_{DM} , particle mass m_{DM} , and radius R_{DM} can be roughly mapped to a boson star with total mass M_{BS} and scalar field mass m_{BS} , as long as

$$\frac{M_{\text{DM}}m_{\text{DM}}}{\varpi} \sim \frac{M_{\text{BS}}m_{\text{BS}}}{\hbar}. \quad (70)$$

If we take

$$\varpi \sim \Delta x \Delta p \sim R_{\text{DM}} m_{\text{DM}} \sqrt{GM_{\text{DM}}/R_{\text{DM}}}, \quad (71)$$

Eq. (70) may be rewritten as

$$\frac{M_{\text{DM}}}{M_{\text{BS}}} \sim 5.1 \times 10^{-8} \times \left(\frac{M_{\text{DM}}}{M_{\odot}}\right)^{1/2} \left(\frac{R_{\text{DM}}}{10^6 R_{\odot}}\right)^{1/2} \left(\frac{m_{\text{BS}}c^2}{10^{-23}\text{eV}}\right). \quad (72)$$

With the mapping established between a DMC and a boson star, we can then discuss the relation between their perturbative properties. The tidal deformability λ , for example, can be obtained by first computing the rescaled (dimensionless) quantity $\tilde{\lambda} := (mc/\hbar)^5 \lambda$, and then restoring the physical dimensions to obtain the final value. This indicates that

$$\lambda_{\text{DM}} \sim \lambda_{\text{BS}} \left(\frac{m_{\text{DM}}\hbar}{m_{\text{BS}}\varpi}\right)^{-5} \sim \lambda_{\text{BS}} \left(\frac{M_{\text{DM}}}{M_{\text{BS}}}\right)^5. \quad (73)$$

In particular, for dark matter clumps, the tidal Love number $k_{\text{DM}} := \lambda(GM_{\text{DM}}/c^2)^5$, defined in analogy with Eq. (56), is given by [cf. Eq. (66)]

$$k_{\text{DM}} = 1149 \times \left(\frac{\varpi}{m_{\text{DM}}c}\right)^{10} \sim 1149 \times \left(\frac{GM_{\text{DM}}R_{\text{DM}}}{c^2}\right)^5 \quad (74)$$

where again we used Eq. (71).

Other perturbative properties, such as the quasinormal mode frequencies of oscillations, allow for analogous mappings. We can first evaluate the rescaled mode frequency for the rescaled equation, Eq. (68), and then scale it back to original configurations. At the end, the mode frequencies are (approximately) related by

$$\omega_{\text{DM}} \sim \omega_{\text{BS}} \left(\frac{m_{\text{DM}}\hbar}{m_{\text{BS}}\varpi}\right) \sim \omega_{\text{BS}} \left(\frac{M_{\text{BS}}}{M_{\text{DM}}}\right). \quad (75)$$

Thus, results obtained for the quasinormal modes of boson stars [29, 30] can be translated into estimates for cold dark matter clumps.

We notice that after a stationary boson star configuration is mapped to a DMC, it generally does not remain stationary, as the underlying evolution equation becomes the collisionless Boltzmann equation instead of the Moyal equation. However, due to the close proximity between these two equations, as discussed in Sec. II and Sec. III, it is possible that the DMC just oscillates around a new equilibrium configuration, which is not far from its initial state. In this case, the oscillation frequency and tidal deformability of the new equilibrium configuration should be roughly consistent with the numbers we obtain by analyzing the perturbations of the original boson star. In the future, it would be interesting to test this claim with further numerical experiments.

V. CONCLUSION

In this work, we discuss an approximate method to analyze the dynamical behaviour of dark matter clumps, in which the phase-space density distribution of the dark matter particles, which follows the (collisionless) Boltzmann equation, is traded by a Wigner quasiprobability distribution following the Moyal equation. Equivalently, the problem can be formulated in terms of wave functions evolving according to a set of coupled Schrödinger-Poisson equations. In contrast to previous treatments, where many short-wavelength wave functions were required in order to reduce the error in approximating the Boltzmann equation, here we work in the regime where the effective particle wavelength is comparable to the spatial variation scale of the phase-space distribution. We discuss the error incurred in adopting this procedure, and illustrate through a numerical simulation that the relative error from the difference in the evolution equations is small within dynamical timescales.

There are many advantages associated with a (approximate) dual wave description. First of all, wave functions are three dimensional, so that much lower computation cost is required to simulate the wave evolution than solving a (six-dimensional) Boltzmann equation. Second, a wave description is specially convenient for analytical and perturbative analyses, which also help us build physical intuition into the system. Finally, this wave analogy provides us a link to compare the phenomenology of cold DM

models and scalar wave DM models, while their mass scales usually differ by many orders of magnitude.

To illustrate these points, in this work we performed a calculation of the tidal deformability of relativistic boson stars, and use it to infer similar properties for DMCs. Although such identification is only approximate, it still offers a useful method to describe the perturbative behaviour (encoded in quantities such as the tidal Love number, quasinormal modes, etc.) of generic DMCs.

Acknowledgments

HY thanks Haixing Miao and Ue-Li Pen for very instructive discussions. We thank Eric Poisson for reading

over a draft of this manuscript and giving many useful comments. R.M. acknowledges financial support from Conselho Nacional de Desenvolvimento Científico e Tecnológico (CNPq). H. Y. acknowledges support from the Perimeter Institute for Theoretical Physics and the Institute for Quantum Computing. Research at Perimeter Institute is supported by the government of Canada and by the Province of Ontario through Ministry of Research and Innovation.

-
- [1] G. Steigman, B. Dasgupta, and J. F. Beacom, *Phys. Rev. D* **86**, 023506 (2012).
- [2] J. M. Gaskins (2016), 1604.00014.
- [3] M. Ackermann, A. Albert, B. Anderson, W. B. Atwood, L. Baldini, G. Barbiellini, D. Bastieri, K. Bechtol, R. Bellazzini, E. Bissaldi, et al. (The Fermi-LAT Collaboration), *Phys. Rev. Lett.* **115**, 231301 (2015).
- [4] V. Springel, S. D. M. White, A. Jenkins, C. S. Frenk, N. Yoshida, L. Gao, J. Navarro, R. Thacker, D. Croton, J. Helly, et al., *Nature* **435**, 629 (2005).
- [5] B. Moore, *Nature* **370**, 629 (1994).
- [6] M. Mateo, *Ann. Rev. Astron. Astrophys.* **36**, 435 (1998).
- [7] J. E. Kim, *Phys. Rev. Lett.* **43**, 103 (1979).
- [8] D. N. Spergel and P. J. Steinhardt, *Phys. Rev. Lett.* **84**, 3760 (2000).
- [9] R. Adhikari, M. Agostini, N. A. Ky, T. Araki, M. Archidiacono, M. Bahr, J. Behrens, F. Bezrukov, P. B. Dev, D. Borah, et al. (2016), 1602.04816.
- [10] H.-Y. Schive, T. Chiueh, and T. Broadhurst, *Nature Physics* **10**, 496 (2014).
- [11] V. S. Berezhinsky, V. I. Dokuchaev, and Y. N. Eroshenko, *Physics-Uspekhi* **57**, 1 (2014).
- [12] E. W. Kolb and I. I. Tkachev, *Phys. Rev. D* **50**, 769 (1994).
- [13] C. Schmid, D. J. Schwarz, and P. Widerin, *Phys. Rev. D* **59**, 043517 (1999).
- [14] J. Silk and A. Stebbins, *Astrophys. J.* **411**, 439 (1993).
- [15] E. Bertschinger, *The Astrophysical Journal Supplement Series* **58**, 39 (1985).
- [16] Y. Ali-Haïmoud, E. D. Kovetz, and J. Silk, *Phys. Rev. D* **93**, 043508 (2016).
- [17] B. P. Abbott, R. Abbott, R. Adhikari, P. Ajith, B. Allen, G. Allen, R. S. Amin, S. B. Anderson, W. G. Anderson, M. A. Arain, et al. (LIGO Scientific Collaboration), *Rep. Prog. Phys.* **72**, 076901 (2009).
- [18] P. Amaro-Seoane, S. Aoudia, S. Babak, P. Binétruy, E. Berti, A. Bohé, C. Caprini, M. Colpi, N. J. Cornish, K. Danzmann, et al., *GW Notes* **6**, 4 (2013).
- [19] B. P. Abbott, R. Abbott, T. D. Abbott, M. R. Abernathy, F. Acernese, K. Ackley, C. Adams, T. Adams, P. Addesso, R. X. Adhikari, et al. (LIGO Scientific Collaboration and Virgo Collaboration), *Phys. Rev. Lett.* **116**, 061102 (2016).
- [20] M. Armano, H. Audley, G. Auger, J. T. Baird, M. Bassan, P. Binétruy, M. Born, D. Bortoluzzi, N. Brandt, M. Caleno, et al., *Phys. Rev. Lett.* **116**, 231101 (2016).
- [21] P. J. E. Peebles, *The large-scale structure of the universe* (Princeton University Press, Princeton, N.J., 1980).
- [22] P. J. E. Peebles, *Astrophys. J.* **317**, 576 (1987).
- [23] L. M. Widrow and N. Kaiser, *The Astrophys. J.* **416**, L71 (1993).
- [24] M. Schaller, C. Becker, O. Ruchayskiy, A. Boyarsky, and M. Shaposhnikov, *Mon. Not. Roy. Astr. Soc.* **442**, 3073 (2014).
- [25] L. M. Widrow and N. Kaiser, *The Astrophys. J.* **485**, 484 (1997).
- [26] P. Jetzer, *Phys. Rep.* **220**, 163 (1992).
- [27] F. E. Schunck and E. W. Mielke, *Classical Quantum Gravity* **20**, R301 (2003).
- [28] S. L. Liebling and C. Palenzuela, *Living Rev. Relativity* **15**, 6 (2012).
- [29] S. Yoshida, Y. Eriguchi, and T. Futamase, *Phys. Rev. D* **50**, 6235 (1994).
- [30] C. F. B. Macedo, P. Pani, V. Cardoso, and L. C. B. Crispino, *Phys. Rev. D* **88**, 064046 (2013).
- [31] H. Yang, H. Miao, D.-S. Lee, B. Helou, and Y. Chen, *Phys. Rev. Lett.* **110**, 170401 (2013).
- [32] M. O. Scully and M. S. Zubair, *Quantum Optics* (Cambridge University Press, 1997).
- [33] G. S. Agarwal, *Quantum Optics* (Cambridge University Press, 2013).
- [34] A. Zee, *Quantum field theory in a nutshell* (Princeton University Press, 2010).
- [35] L. Diosi, *Phys. Lett. A* **105**, 199 (1984).
- [36] P. Coles and K. Spencer, *Mon. Not. Roy. Astr. Soc.* **342**, 176 (2003).
- [37] N. Stone, R. Sari, and A. Loeb, *Mon. Not. Roy. Astr. Soc.* **435**, 1809 (2013).
- [38] L. M. Widrow, *Phys. Rev. D* **55**, 5997 (1997).
- [39] E. Poisson and C. Will, *Gravity: Newtonian, post-Newtonian, Relativistic* (Cambridge University Press, England, 2014).
- [40] K. S. Thorne, *Phys. Rev. D* **58**, 124031 (1998).
- [41] T. Hinderer, *Astroph. J.* **677**, 1216 (2008).